Evolution from point to extended defects in ion implanted silicon

J. L. Benton,[a] S. Libertino,[b] P. Kringhøj,[c] D. J. Eaglesham, and J. M. Poate[d]
Bell Laboratories, Lucent Technologies, 600 Mountain Avenue, Murray Hill, New Jersey 07974

S. Coffa
CNR-IMETEM, Stradale Primosole 50, I-95121 Catania, Italy

(Received 25 November 1996; accepted for publication 24 March 1997)

We present a quantitative study of the evolution of point defects into clusters and extended defects in ion-implanted Si. Deep level transient spectroscopy (DLTS) measurements are used to identify and count the electrically active defects in the damaged region produced by Si ion implantation at energies of 145 keV–2 MeV, and fluences from 1×10^{8} to 5×10^{13} Si/cm^2. Analyses of silicon annealed in the temperature range 100–680 °C allow us to monitor the transition from simple point defects to defect clusters and extended defects that occur upon increasing the ion fluence and the annealing temperature. At low doses, $<10^{10}$ Si/cm^2, only about 2% of the Frenkel pairs generated by the ion beam escape recombination and are stored into an equal number of interstitial and vacancy-type point defects. Thermal treatments produce a concomitant annealing of interstitial and vacancy-type defects until, at temperatures above 350 °C, only two to three interstitial-type defects per ion are left, and the DLTS spectra contain signatures of second-order point defects. Interstitial clusters at $E_v+0.29$ and $E_v+0.48$ eV are found to dominate the residual damage of silicon implanted at higher fluences, 1×10^{12}–7×10^{13} Si/cm^2, and at annealing temperatures, $T\geqslant600$ °C. These interstitial clusters have point defect capture kinetics and are not observable in transmission electron microscopy (TEM), suggesting that they are smaller than ≈50 Å. Finally, for silicon implanted at higher Si doses, $\geqslant5\times10^{13}$ Si/cm^2, thermal treatments at 680 °C result in a strong decrease in the concentration of the interstitial cluster signatures and in the introduction of a different DLTS signal, $E_v+0.50$ eV, which exhibits logarithmic rather than exponential carrier capture kinetics, a feature typical of an extended defect. Comparison of the formation and dissolution of this extended defect signature with TEM analyses indicates that this level is a signature of the rodlike {311} defects that are known to store the interstitials responsible for transient enhanced diffusion. These results suggest that the small interstitial clusters are either the precursors of the {311} defects or that they compete with {311} defects as sinks for self-interstitials. © *1997 American Institute of Physics.* [S0021-8979(97)00413-1]

I. INTRODUCTION

Ion implantation is a standard processing step in the manufacturing of very-large scale integrated (VLSI) Si devices. Quantitative information on damage evolution upon annealing of ion-implanted crystalline Si is crucial for the understanding and correct modeling of numerous phenomena, such as the formation of extended defects[1,2] and transient enhanced diffusion.[3–5] The new generation of simulation tools for the design of submicron devices require an accurate scientific description of defect–defect and defect–impurity interaction during the various implantation and annealing processes. In spite of this large scientific and technological interest in ion-implanted material, most of our current knowledge of defect structure and annealing behavior still relies on the detailed studies performed during the last 20 years on electron irradiated samples.[6–11] Techniques sensitive to point defects and small defect clusters, such as deep level transient spectroscopy (DLTS), photoluminescence, (PL), or electron paramagnetic resonance (EPR), have been used in these studies to identify the room temperature stable point defect structures and their annealing behavior. Such detailed knowledge is missing for ion-implanted Si. In fact, while several investigations[12–14] have focused on determining the defect structure of the as-implanted samples in the low dose limit, no quantitative evaluation of defect evolution with temperature has yet been presented.

Furthermore, the high implantation fluences (typically higher than 10^{13} cm^{-2}) used in device fabrication are outside the domain usually explored by DLTS and PL. In this domain, damage evaluation has been traditionally obtained with techniques such as Rutherford backscattering spectrometry (RBS) and transmission electron microscopy (TEM). Although extremely powerful, these techniques fail to monitor small defect clusters. It is, therefore, extremely difficult to link the results of the different techniques into a coherent picture. The question of how the simple defect structures evolve into more complex structures or even into extended defects, upon increasing ion fluence and annealing temperature, still remains unanswered.

[a]Electronic mail jlb@bell-labs.com
[b]Permanent address: INFM and Dipartimento di Fisica, Università di Catania, Corso Italia 57, I95129 Catania, Italy.
[c]Permanent address: Institute of Physics and Astronomy, Aarhus University, DK-8000 Aarhus C, Denmark.
[d]Current address: New Jersey Institute of Technology, 504 Cullimore Hall, University Heights, Newark, NJ 07102.

 0021-8979/97/82(1)/120/6/$10.00

A. Radiation-induced point defects

The interstitials and the vacancies generated by high energy ion beams are mobile at room temperature and, therefore, they undergo extensive recombination, defect clustering, and formation of pairs with impurity and dopant atoms of the substrate. These phenomena result in the introduction of room temperature stable defect complexes and defect-impurity pairs. The hierarchy of these defect complexes has been well characterized for electron irradiated samples while such a systematic study is lacking in ion-implanted material.

Over the past 20 years, detailed capacitance transient analyses of electron-beam irradiated Si (Refs. 6–11) have fully characterized the production of interstitial-vacancy Frenkel pairs and the migration of Si interstitials to dopant or impurity atoms where interstitial impurities such as B_i and C_i are created by the Watkins exchange mechanism.[15] These interstitial species subsequently diffuse at room temperature until they are trapped, forming interstitial-impurity pairs such as carbon–carbon (C_s-C_i), carbon–oxygen, (C_i-O_i), or boron–boron, (B_i-B_s).[7,8,16–18] In a similar manner, vacancies also migrate through the Si lattice and cluster or pair with impurities to create point defects such as divacancies, ($V-V$), vacancy–oxygen, ($V-O$), or vacancy–phosphorus ($V-P$).[9–11] All these simple point defect pairs anneal at well characterized temperatures below 450 °C.

In *n*-type Si, defects with states in the upper half of the band gap, $O-V$, $E(0.17\ \text{eV})$, two charge states of $V-V$, $E(0.23\ \text{eV})$ and $E(0.40\ \text{eV})$, and $P-V$, $E(0.44\ \text{eV})$, are normally observed in DLTS after electron irradiation. In silicon with a high concentration of carbon, signals related to P_s-C_i, $E(0.29\ \text{eV})$, and C_s-C_i, $E(0.17\ \text{eV})$, have also been identified. In *p*-type Si, the third charge state of the $V-V$, $H(0.23\ \text{eV})$, the B_iC_s, $H(0.26\ \text{eV})$ and the C_i-O_i, $H(0.36\ \text{eV})$, signatures are seen. The introduction rates and annealing kinetics of these point defect pairs are well characterized and are known to depend critically on the relative concentrations of dopant atoms, oxygen, and carbon in the starting material. The wealth of published information on the identity, introduction rates, annealing behavior, and DLTS signatures of vacancy and interstitial related point defects in electron irradiated Si provides a firm foundation for a comprehensive study of the introduction and evolution of implantation-induced defects in Si.

Certainly ion implantation has some inherent differences compared to electron irradiation. First, the defect profile is not spatially uniform but, rather, is generally distributed in a well defined peak at the end of range. Second, the density of collisional events is several orders of magnitude higher in ion-irradiated material, resulting in high density collision cascades, and favoring defect clustering. Finally, the Frenkel pair generation of an equal number of vacancies and interstitials is unbalanced by the displacement of the target atom and by the incorporated extra ions. This last observation has noticeable consequences and provides the basis for the +1 model[19] that is used to describe high fluence, high temperature annealing phenomena. In this model, it is assumed that extensive recombination of vacancies and interstitials occurs until only the extra ion is left.

B. Ion-implantation induced extended defects

Just as there is a body of experiments detailing the introduction and structure of point defects in ion-implanted Si in low damage regimes, there is also a detailed understanding of extended interstitial defects created by high dose ion-implantation or thermal oxidation.[2,20–22] The structural properties of these ''rodlike'' or {311} defects have been determined by TEM. Recently it has been proven that the injection of interstitials from the dissolution of {311} defects during annealing at 670–815 °C drives the technologically important phenomenon of transient enhanced dopant diffusion.[23] The work reported in this article provides the ''missing link''[24] between the well characterized regimes of point defect formation at low interstitial concentrations and extended defect formation at much higher interstitial concentrations.

Until now, simulations rather than experimental evidence have provided the only quantitative description of damage evolution from Frenkel pair generation to extended defects.[25,26] Semi-empirical fits to the experimentally observed interstitial clustering ({311} defects) have successfully reproduced the phenomena of extended defect formation and dissolution.[23] Models generally need to invoke only strong interstitial–interstitial and vacancy–vacancy binding to reproduce the clustering. Furthermore, most reasonable choices of binding energies and diffusivities will reproduce the ''plus one'' observations. Several hints as to the physical mechanisms involved in defect growth have resulted from simulations of model studies. For example, interstitial clusters have been clearly identified as the primary factor in damage evolution upon annealing, and the importance of the extra implanted ion has been defined. Clearly much more experimental work as well as validation of simulation tools is mandatory for a thorough comprehension of this complex phenomenon.

In this article we provide a quantitative evaluation of ion-implantation induced damage evolution by monitoring the concentrations of interstitial- and vacancy-type defects from the as-implanted configuration through heat treatments up to 700 °C for wide variations of ion fluences and thermal processes. The implications of these results on the current understanding of the defect structure of ion-implanted crystalline Si are discussed.

II. EXPERIMENT

The Si samples used for these experiments were both *n* type and *p* type with a wide range of resistivities, 0.1–10 Ω cm. Crucible-grown Czochraiski (CZ) and epitaxial grown (epi) substrates were investigated. Implant doses ranged from 3×10^8 to 7×10^{13} Si/cm^2 at implant energies of 145 keV–2 MeV. Schottky barriers were deposited at room temperature to form measurement structures using AuPd for *n*-type diodes and Ti for *p* type. The resistivities of the samples were chosen to allow the depletion region of the reversed biased Schottky barriers to sweep through the range of the implanted species. Defect identities, concentrations, and depth profiles were measured by a BioRad DL8000 DLTS spectrometer, and all spectra presented in this work were mea-

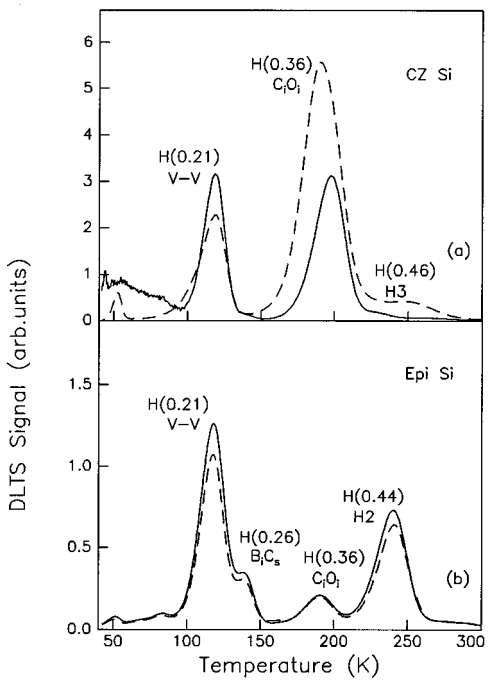

FIG. 1. Comparison of DLTS defect spectra, τ=9 ms, in p-type silicon for electron irradiation and Si ion implantation. (a). Defect signatures in CZ material resulting from 9.2 MeV, 1×10^{15} e^-/cm^2 (solid line) and 2 MeV, 3×10^8 Si/cm^2 (dashed line). The slight differences in the relative defect concentrations reflect different oxygen concentrations in the two substrates, (b) Defect spectra in epitaxial Si after irradiation with 1.2 MeV, 1×10^9 Si/cm^2 (dashed line), and with 9.2 MeV, 3.5×10^{15} e^-/cm^2 (solid line).

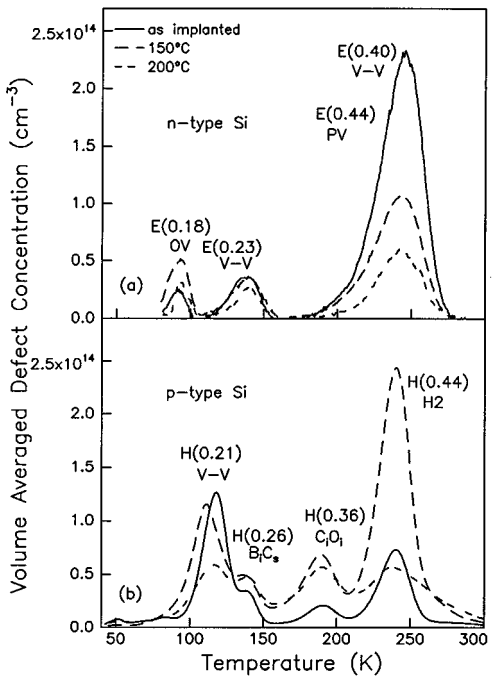

FIG. 2. DLTS defect spectra, τ=9 ms, in (a) n-type and (b) p-type epitaxial Si implanted with 1.2 MeV, 1×10^9 Si/cm^2. The as-implanted samples exhibit the well known point defect pairs (solid lines), and the spectra measured after 30 min at T=150 and 200 °C show the anneal of interstitial- and vacancy-related defects.

sured with an instrument time constant, τ=9 ms. Anneals at temperatures ranging from 100 to 685 °C were performed in a tube furnace using a He ambient.

III. RESULTS AND DISCUSSION

A. Introduction and thermal evolution of point defects

We will first analyze the defect structure of Si implanted at low fluences, $<10^{10}$ Si/cm^2, which allows us to follow the defect evolution upon annealing from room temperature to 400 °C. Recent comparisons of n-type Si after either MeV electron irradiation or low dose Si ion implantation show identical DLTS defect spectra with the exception of the relative concentrations of the two charge states of $V-V$.[27] Similar comparisons of defect formation in p-type Si have not previously been published, but here we show that identical defect pairs are created by the processes.

Figure 1 compares the DLTS spectra for Si ion-implanted material with electron irradiated samples for both CZ and epitaxial, p-type Si samples that both show the signatures of the $V-V$, $H(0.21\ \mathrm{eV})$ and the C_iO_i, $H(0.36\ \mathrm{eV})$. The doses and energies were chosen to give the same defect concentrations for electron and ion introduction in the measurement volume. The chemical identity of the defect signature $H(0.46\ \mathrm{eV})$ has not yet been determined. Although the spectra are identical for both electron and ion irradiation on the same substrates, there is an obvious difference in defect production as a function of impurity concentrations in the various substrates. The epitaxial p/p^+ wafers used in these examples have very low impurity concentrations with $[\mathrm{O}]\approx10^{15}\ \mathrm{cm}^{-3}$ and $[\mathrm{C}]\leqslant10^{15}\ \mathrm{cm}^{-3}$, and therefore, show a low concentration of C_i-O_i pairs. Two additional defect signals are present at room temperature, B_iC_s, $H(0.26\ \mathrm{eV})$ and $H2(0.44\ \mathrm{eV})$, which are not seen in the as-implanted CZ samples at room temperature but which do appear with further heat treatment at 150 °C. The difference in the formation temperature of B_iC_s is a consequence of the difference in the C concentrations in the epitaxial and CZ Si. Interstitials created by the irradiation diffuse at room temperature and preferentially form B_i by the Watkins exchange mechanism[15] in the epitaxial Si rather than the C_i formed in the CZ Si, $[\mathrm{C}]=10^{16}\ \mathrm{cm}^{-3}$. Thus in epitaxial Si, the mobile B_i pairs with C_s to create B_iC_s, whereas in CZ Si this defect forms after the dissociation of C_i-related complexes. $H2(0.44\ \mathrm{eV})$ has been tentatively identified as an interstitial-type defect containing B.[28]

In order to understand the evolution of the point defects in Si ion-implanted Si, samples were monitored after isochronal anneals in 50 °C steps from 100 to 400 °C. Spectra taken on the low carbon p/p^+ and n/n^+ epitaxial Si are plotted in Fig. 2, comparing the 1.2 MeV, 1×10^9 Si/cm^2 as-implanted results after 30 min anneals at 150 and 200 °C. The total point defect concentration is reduced by an order of magnitude after 350 °C thermal treatments. The n-type samples show the signatures of the OV, $E(0.18\ \mathrm{eV})$, and the PV, $E(0.44\ \mathrm{eV})$ and two charge states of the $V-V$, $E(0.23\ \mathrm{eV})$ and $E(0.40\ \mathrm{eV})$. Annealing at 150 °C produces a reduction in the concentration of the

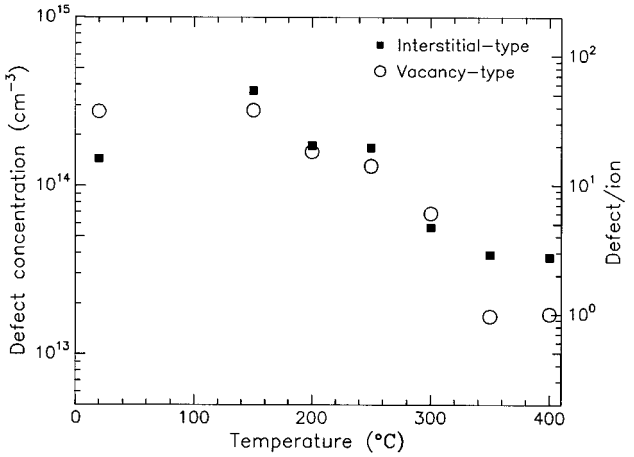

FIG. 3. Isochronal anneals for 30 min that compare the total interstitial-type defect concentration (square data points) with the total vacancy-type defect concentrations (round data points) in 1.2 MeV, 1×10^9 Si/cm^2 ion-implanted, epitaxial Si. A balance of interstitials and vacancies is maintained until $T\geqslant350$ °C, when the remaining defects are interstitial complexes.

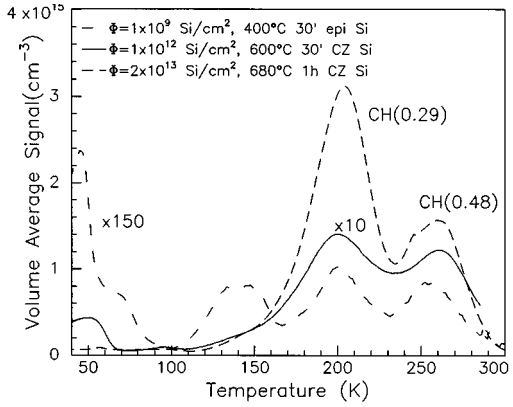

FIG. 4. Second-order defect signals are measured by DLTS in epitaxial Si, 1.2 MeV, 1×10^9 Si/cm^2, 400 °C, 30 min (short-dashed line) after the anneal of point defect pairs. Broad DLTS signatures of interstitial cluster defects then evolve, as shown in the examples of *p*-type CZ Si after 1.2 MeV, 1×10^{12} Si/cm^2, 600 °C, 30 min (solid line), and epitaxial Si, 145 keV, 2×10^{13} Si/cm^2, 680 °C, 30 min (dashed line).

high temperature DLTS peak, which corresponds to the anneal of PV pairs.

Important insights into the evolution of interstitial defects in ion-implanted Si can be gained by analysis of both the vacancy- and interstitial-related defect signals which can be quantitatively measured with DLTS as a function of annealing temperature. The concentration of vacancies stored in vacancy-related defects is the sum of $[VO]+2[V-V]$; the concentration of interstitials stored in interstitial-related defects is the sum of $[C_iO_i]+[B_iC_s]+[H(0.44)]$. For annealing temperatures >300 °C, no vacancy-type defect signatures are found, and we have assumed that all the residual damage is of the interstitial type. The results of this calculation are summarized in Fig. 3 for 1.2 MeV, 1×10^9 Si/cm^2 ion-implanted, epitaxial Si. Several interesting conclusions can be derived from Fig. 3. First, in the as-implanted condition, an almost equal number of interstitial- and vacancy-type defects is contained in the electrically active complexes. This number is approximately 60 per implanted ion. Since, according to TRIM,[29] (transport of ion in matter, a Monte Carlo code), about 2500 Frenkel pairs are generated by the Si ion beam, this result implies that only ~2–3% of these elementary defects escape recombination. Furthermore, vacancy-type and interstitial-type defects anneal concurrently, and an identical annealing behavior, $T\leqslant300$ °C, is measured for both of these two kinds of defects. However at $T\approx350$ °C, only interstitial-type defects remain, and their concentration corresponds to two to three interstitials per implanted ion, a number quite close to the net excess of interstitials predicted by the +1 model.[19]

These results have noticeable consequences. The concomitant annealing of vacancy- and interstitial-type defects can be understood by assuming, for example, that the anneal of vacancy-type complexes releases free vacancies that then anneal interstitial-type defects. This implies that recombination of free defects at the surface is not the dominant annihilation mechanism and that the balance of interstitials and vacancies is maintained until most of them are recombined. At this point, $T\approx350$ °C, only interstitial clusters appear to survive which is consistent with Monte Carlo simulations of diffusion and experimental investigations that indicate that vacancy clusters are less stable than interstitial clusters.[9–11,26]

B. Formation of interstitial clusters

Upon continued annealing, interstitial point defects are expected to agglomerate in an Ostwald ripening process to form small clusters, although there is no experimental evidence of these clusters. Our investigations by DLTS of a wide range of Si implant doses and annealing temperatures has produced electrical signatures related to interstitial cluster defects.

The introduction of point defects is observed in the ion fluence range from 1×10^8 to 5×10^9 Si/cm^2. At fluences greater than 5×10^9 Si/cm^2, the concentration of defects is higher than the concentration of dopants and, therefore, quantitative evaluation of the ion-induced defects in the as-implanted state is not possible by DLTS. However, it is possible to analyze the defects that occur after annealing at elevated temperatures >400 °C. We have monitored samples implanted with increasing doses, $1\times10^9-5\times10^{13}$ Si/cm^2 at annealing temperatures 400–680 °C and note that, when the increase in the ion fluence is accompanied by an increase in the annealing temperature, similar DLTS signatures are observed in the residual damage. Typical spectra are shown in Fig. 4 for three samples receiving widely varying implant doses and annealing temperatures: a *p*-type, CZ silicon substrate implanted at 145 keV, 2×10^{13} Si/cm^2 and given heat treatment of 685 °C, 1 h; another CZ sample implanted at 1.2 MeV 1×10^{12} Si/cm^2, with a 600 °C, 30 min anneal; and an epi sample implanted at 1.2 MeV 1×10^9 Si/cm^2, with anneal of 400 °C, 30 min. The total defect concentration scales with the Si implant dose.

The DLTS spectrum in Fig. 4 corresponding to a dose of 1×10^9 Si/cm^2 (short-dashed line) shows numerous signatures related to new second-order point defects which form

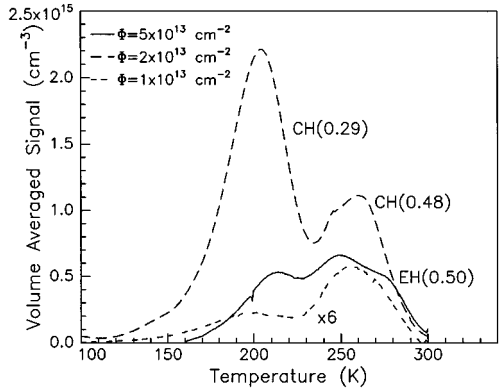

FIG. 5. DLTS spectra after 145 keV Si ion implantation and thermal anneal of 685 °C, 1 h. The concentration of cluster defects increases as the dose is raised from 1×10^{13} to 2×10^{13} Si/cm^2. At a fluence of 5×10^{13} Si/cm^2, the total concentration of cluster defects is dramatically reduced and the extended defect signature, EH(0.50 eV), is observed.

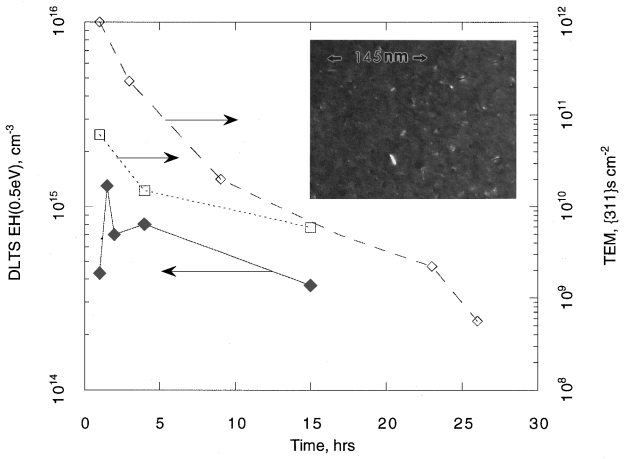

FIG. 6. The concentration of {311} defects determined by plan-view TEM (right axis, open data points) compared to the concentration of extended defects, EH(0.50 eV), measured by DLTS (left axis, solid data points) for the same sequence of isothermal anneals. The ion implantation was 5×10^{13} Si/cm^2 at 145 keV for the DLTS (solid line) and TEM (short-dashed line), and at 40 keV for the additional TEM series (dashed line). The inset is a TEM micrograph of the {311} defects in the sample used for DLTS after a 1 h anneal at 680 °C.

upon anneal of the point defect pairs. The physical identity of these defects has not been determined, but similar sets of DLTS signatures are observed following 1.2 MeV implantation at doses $1\times10^{9}-1\times10^{12}$ Si/cm^2 after 30 min heat treatments, 400 °C$\leqslant T\leqslant$500 °C.

At higher doses, $1\times10^{12}-7\times10^{13}$ Si/cm^2 (Fig. 4, solid and dashed lines), and higher temperatures, $T\geqslant$600 °C, two signatures, CH(0.29) and CH(0.48), dominate the DLTS spectra. This is an intriguing result, and it suggests that the signatures could relate to particularly stable defect structures. It is important to note that these two spectral peaks as shown in Fig. 4 are wider than is characteristic for point defect signals, suggesting that these defects are small clusters. Hole capture kinetics for both levels are exponential, and no extended defects are observable in plan view TEM. These three pieces of experimental evidence lead to an initial identification of these two DLTS peaks as interstitial clusters smaller than 50 Å. In order to distinguish the DLTS defect signatures of clusters from the signals of point defects, we have modified the standard convention of indicating an activation energy for hole emission from the deep level in the band gap to the valance band from H() to CH(). These two cluster defects are therefore identified as CH(0.29 eV) and CH(0.48 eV) It is surprising to observe a single set of defect signals over such a wide range of dose and temperatures in view of the Monte Carlo simulations which predict the continual formation of interstitial atomic clusters of increasing size.

C. Observation of extended defects

For implant fluences $\geqslant5\times10^{13}$ Si/cm^2, a new regime is entered, characterized by the formation of extended defects which are observed by both DLTS and TEM analysis. A 145 keV Si ion implant dose of 5×10^{13} Si/cm^2 plus a heat treatment of 685 °C, 1 h, produces {311} defects. DLTS spectra for a Si sample subjected to this recipe as well as for samples given lower doses of 1×10^{13} and 2×10^{13} Si/cm^2 are displayed in Fig. 5. Two important spectral changes occur as the Si fluence is increased to the regime that produces {311} defects. There is a decrease in the concentration of the signals related to the cluster defects, CH(0.29) and CH(0.48), and there is additional defect signal, seen as a high temperature shoulder on CH(0.48 eV). Deconvolution of the spectral peaks yields a tentative energy for thermally stimulated carrier emission of EH(0.50 eV). Following our convention, extended defects are labeled EH(). The hole capture kinetics of this defect signal were experimentally determined by varying the filling pulse width, and display a logarithmic dependence, which is the identifying characteristic of an extended defect.[30,31] Plan-view, dark field, TEM micrographs (a typical micrograph is shown as an inset in Fig. 6) show that {311} defects are present in the samples where the EH(0.50 eV) signature is observed by DLTS and that the {311} defects are not visible in the lower dose samples, which display only the signals that are related to the interstitial clusters. This suggests that the broad shoulder in the DLTS spectra is a signature of the {311} defects. Additional support for this idea is gained by comparing the kinetics of formation and dissociation of the DLTS signature with TEM observations of the {311} defects.

The ion-implantation regime of Si doses ranging from 5×10^{12} to 1×10^{14} Si/cm^2 has been extensively studied by transmission electron microscopy. The damage evolves into a distribution of interstitial agglomerates, known as {311} defects after heat treatments of 670–815 °C.[23] The concentration of these agglomerates decreases while their size increases in an Ostwald ripening process, accompanied by the emission of interstitials from the defects. The density of {311} defects seen in plan-view TEM data is compared with the DLTS measurement of the EH(0.50 eV) concentration for the same series of isothermal anneals for samples implanted with 145 keV, 5×10^{13} Si/cm^2 (Fig. 6, solid line is DLTS extended defect concentrations and the short-dashed line is the {311} density measured by TEM), and the density of {311} defects measured by TEM for samples implanted

with 40 keV, 5×10^{13} Si/cm^2 (dashed line). The defect concentrations measured by DLTS for this comparison were taken from the maximum peak height with no correction for the extended nature of the defect signals, so, therefore, give a lower limit on the number of defects. These data are consistent with a link between the extended defect signals in DLTS and the {311} defects measured by TEM and provide observations of an electrical signature related to the presence of {311} defects created by ion beam processing.

Finally, noting that the formation of {311} defects significantly suppresses the concentration of the defect clusters, CH(0.29) and CH(0.48), suggests that either CH(0.29) and CH(0.48) are signatures of particular interstitial clusters that are the precursors of the {311} defects or that these interstitial clusters compete with {311} defects as sinks for the self-interstitials.

IV. CONCLUSIONS

This extensive survey of the ion implantation damage-related defects created by a range of Si doses covering six orders of magnitude has produced comprehensive experimental evidence of the evolution of interstitial defects from simple pairs to extended {311} defects. The interstitial and vacancy pairs produced by ion implantation are influenced by the impurity concentrations in the silicon and evolve into second-order point defects after low temperature thermal treatments, $350\ ^\circ\text{C}\leqslant T\leqslant 500\ ^\circ\text{C}$. At higher temperatures, $T\geqslant 600\ ^\circ\text{C}$, and at higher doses, $1\times10^{12}-5\times10^{13}$ Si/cm^2, the interstitial defects form small clusters with two associated DLTS signatures, CH(0.29 eV) and CH(0.48 eV). An additional signature of an extended defect, EH(0.50 eV), is correlated to the presence of the {311} structures which are known to supply the interstitials responsible for transient enhanced diffusion of B in Si.

ACKNOWLEDGMENTS

The authors would like to thank and acknowledge the contributions of D. C. Jacobson for his supervision of the ion implantations, P. G. Fuochi and M. Lavalle for the electron irradiations, and N. Parasole for expert technical assistance.

[1] M. Tamura, N. Natsuaki, Y. Wada, and E. Mitani, Nucl. Instrum. Methods Phys. Res. B **21**, 438 (1987).
[2] K. S. Jones, S. Prussin, and E. R. Weber, Appl. Phys. A **45**, 1 (1988).
[3] P. A. Stolk, H. J. Gossmann, D. J. Eaglesham, D. C. Jacobson, J. M. Poate, and H. S. Luftman, Appl. Phys. Lett. **66**, 568 (1995).
[4] H. J. Gossmann, C. S. Rafferty, H. S. Luftman, F. C. Underwald, T. Boone, and J. M. Poate, Appl. Phys. Lett. **63**, 639 (1993).
[5] N. E. B. Cowern, K. T. F. Janssen, and H. F. F. Jos, J. Appl. Phys. **68**, 6191 (1990).
[6] L. C. Kimerling, Inst. Phys. Conf. Ser. **31**, 221 (1977).
[7] M. T. Asom, J. L. Benton, R. Sauer, and L. C. Kimerling, Appl. Phys. Lett. **51**, 256 (1987).
[8] J. L. Benton, M. T. Asom, R. Sauer, and L. C. Kimerling, Mater. Res. Soc. Symp. Proc. **104**, 85 (1988).
[9] G. D. Watkins and J. W. Corbett, Phys. Rev. **121**, 1001 (1961).
[10] P. M. Mooney, L. J. Cheng, M. Sull, J. D. Gerson, and J. W. Corbett, Phys. Rev. B **15**, 3836 (1977).
[11] J. W. Corbett and G. D. Watkins, Phys. Rev. A **138**, 555 (1965).
[12] B. G. Svensson, C. Jagadish, A. Hallen, and J. Lalita, Nucl. Instrum. Methods Phys. Res. B **106**, 183 (1995).
[13] J. Lalita, N. Keskitalo, A. Hallen, C. Jagadish, and B. G. Svensson, Nucl. Instrum Methods Phys. Res. B (in press).
[14] A. Hallen, B. U. R. Sundqvist, Z. Paska, B. G. Svensson, M. Rosling, and J. Tiren, J. Appl. Phys. **64**, 1266 (1990).
[15] G. D. Watkins, Phys. Rev. B **12**, 5824 (1975).
[16] P. J. Drevinsky, C. E. Caefer, S. P. Tobin, J. C. Mikkelsen, Jr., and L. C. Kimerling, Mater. Res. Soc. Symp. Proc. **104**, 167 (1988).
[17] P. J. Drevinsky, C. E. Caefer, L. C. Kimerling, and J. L. Benton, in *Proceedings of the International Conference on the Science and Technology of Defect Control in Semiconductors*, edited by K. Sumino (Elsevier Science, North-Holland, 1990), p. 341.
[18] P. J. Drevinsky and H. M. DeAngelis, *Thirteenth International Conference on Defects in Semiconductors*, edited by L. C. Kimerling and J. M. Parsey, Jr. (The Metallurgical Society of AIME, Warrendale, PA, 1985), p. 807.
[19] M. D. Giles, J. Electrochem. Soc. **138**, 1160 (1991).
[20] M. Seibt, J. Imshcweiler, and H.-A. Hefner, Proc. Electrochem. Soc. **94-2**, 720 (1994).
[21] S. Takeda, M. Kohyama, and K. Ibe, Philos. Mag. A **70**, 287 (1994).
[22] D. J. Eaglesham, P. A. Stolk, J.-Y. Cheng, H.-J. Gossmann, T. E. Haynes, and J. M. Poate, Inst. Phys. Conf. Ser. **146**, 451 (1996).
[23] P. A. Stolk, H.-J. Gossmann, D. J. Eaglesham, D. C. Jacobson, C. S. Rafferty, G. H. Gilmer, M. Jaraiz, J. M. Poate, and T. E. Haynes, J. Appl. Phys. **81**, 6031 (1997).
[24] D. C. Johanson and M. A. Edey, *Lucy, The Beginnings of Humankind* (Simon and Schuster, New York, 1981).
[25] M. Jaraiz, G. H. Gilmer, J. M. Poate, and T. D. de la Rubia, Appl. Phys. Lett. **68**, 409 (1996).
[26] C. S. Rafferty, G. H. Gilmer, M. Jaraiz, D. Eaglesham, and H. J. Gossmann, Appl. Phys. Lett. **68**, 2395 (1996).
[27] B. G. Svensson, B. Mohadjeri, A. Hallen, J. H. Svensson, and J. W. Corbett, Phys. Rev. B **43**, 2292 (1991).
[28] S. Libertino, J. L. Benton, S. Coffa, P. Kringhoj, D. J. Eaglesham, and J. M. Poate (unpublished).
[29] J. P. Biersack and L. G. Haggmark, Nucl. Instrum. Methods **174**, 257 (1980).
[30] P. Omling, E. R. Weber, L. Montelius, H. Alexander, and J. Miche, Phys. Rev. B **32**, 6571 (1985).
[31] P. N. Grillot, S. A. Ringel, G. P. Watson, E. A. Fitzgerald, and Y.-H. Xie, Mater. Res. Soc. Symp. Proc. **325**, 159 (1993).